J. Mol. Biol. (1996) **262**, 532–542

JMB

Nitrate Binding to *Limulus polyphemus* Subunit Type II Hemocyanin and its Functional Implications

Bart Hazes[1]*, Karen A. Magnus[2], Kor H. Kalk[1], Celia Bonaventura[3] and Wim G. J. Hol[1]

[1]*Department of Chemical Physics, University of Groningen, Nijenborgh 4 9747 AG Groningen The Netherlands*

[2]*Department of Biochemistry and Department of Physiology and Biophysics, Case Western Reserve University, School of Medicine, 10900 Euclid Avenue, Cleveland, Ohio 44106-4935, USA*

[3]*Marine Biomedical Center School of the Environment Duke University Marine Laboratory, Beaufort, North Carolina 28516, USA*

**Corresponding author*

The horseshoe crab, *Limulus polyphemus*, employs hemocyanin as an oxygen carrier in its hemolymph. This hemocyanin displays cooperative oxygen binding and heterotropic allosteric regulation by protons, chloride ions and divalent cations. Here, we report the crystal structure of *Limulus polyphemus* subunit type II hemocyanin with a nitrate ion bound in the interface of its first and second domains. Interestingly, the nitrate-binding site coincides with the binding site for the allosteric effector chloride. Oxygen-binding data indeed indicate that nitrate, like chloride, reduces the oxygen affinity of this hemocyanin. The observed binding of two distinct anions to a single site suggests that several other anions may also bind at this site. This opens the intriguing possibility that bicarbonate, which is structurally similar to nitrate and closely linked to respiration, can act as an allosteric effector that lowers the oxygen affinity. Such an effect could be another factor in the repertoire of allosteric regulators of this hemocyanin; however, the physiological implications will be a challenge to decipher, since there exists a complex interplay of effects between bicarbonate, chloride, pH and divalent cations.

Keywords: hemocyanin; allosteric regulation; Bohr effect; crystal structure; nitrate binding

Introduction

Arthropodan hemocyanins form hexameric or multi-hexameric quaternary structures that are freely dissolved in the hemolymph. They reversibly bind molecular oxygen at a dinuclear copper site and normally display extensive allosteric regulation properties including cooperativity. The structure of the mono-hexameric hemocyanin of the spiny lobster, *Panulirus interruptus*, was the first one to be elucidated by X-ray diffraction techniques (Gaykema *et al*., 1984; Volbeda & Hol, 1989). That study revealed that the hexameric quaternary structure, which is believed to be the architectural building block of all arthropodan hemocyanins, consists of two trimers with 32 point-group symmetry. The kidney-shaped monomer is further organized in three domains, with the oxygen-binding dinuclear copper site located in the second domain. Hemocyanins with similar functional and spectroscopic properties are also found in molluscs. However, these are very different, both in sequence (Drexel *et al*., 1987; Lang & Van Holde, 1991) and in quaternary structure (Van Bruggen *et al*., 1982) and will not be further discussed here. For reviews on hemocyanins, see Van Holde & Miller (1982), Ellerton *et al*. (1983) and Markl & Decker (1992).

The hemocyanin in the horseshoe crab *Limulus polyphemus* is an example of a multi-hexameric arthropod hemocyanin. It consists of 48 subunits, arranged in an octa-hexameric complex (Lamy *et al*., 1983; Van Heel & Dube, 1994). Eight homologous but immunologically distinct subunit types have been identified in the complex (Brenowitz *et al*., 1981). Each subunit type occupies a unique position in the quaternary structure (Lamy *et al*., 1983) and has characteristic functional properties (Sullivan *et al*., 1974; Brenowitz *et al*., 1984). The oxygen-binding behaviour of the native *Limulus* hemocyanin complex displays cooperative oxygen binding and heterotropic allosteric regulation by protons, chloride ions and divalent cations

Present addresses: B. Hazes, Department of Medical Microbiology and Immunology, 1–41 Medical Sciences Building, University of Alberta, Edmonton, Alberta, T6G 2H7 Canada; W. G. J. Hol, Biomolecular Structure Center, Department of Biological Structure and Howard Hughes Medical Institute, Box 357742, University of Washington, Seattle, WA 98195-7742, USA.

0022–2836/96/390532–11 $18.00/0

(Brouwer *et al*., 1977, 1982; Brouwer & Serigstad, 1989). The effect of protons is to increase oxygen affinity. This is opposite to what is observed in many hemoglobins and hemocyanins and is therefore referred to as the reversed Bohr effect.

Recently, the crystal structures of oxygenated and deoxygenated *L. polyphemus* subunit type II hemocyanin (*Limulus* II) were determined from crystals grown in the presence of 0.5 M NaCl (Hazes *et al*., 1993; Magnus *et al*., 1994). *Limulus* II is known to be capable of forming single hexameric complexes that still show weak cooperativity and allosteric regulation by chloride ions and protons (Sullivan *et al*., 1974; Brenowitz *et al*., 1984). In view of the cooperativity, the oxygenated and deoxygenated structures were anticipated to be different, representing a high-affinity conformation (R-state) and a low-affinity conformation (T-state), respectively. However, the two crystal structures turned out to be virtually identical except for local changes near the oxygen-binding site. This result was explained by oxygen-binding studies that indicated that *Limulus* II, in media that mimic the crystallisation conditions, is fixed in a non-cooperative, low-affinity conformation (unpublished results). This is most likely due to the presence of 0.5 M NaCl in the medium, and in both structures a chloride ion was actually found to bridge the interface between the first and second domains. A similar fixation of a low-affinity, non-cooperative state by chloride is observed in the native 48-meric hemocyanin complex, though at much higher chloride concentrations (Brouwer *et al*., 1982).

A tentative structural model for the allosteric regulation of arthropodan hemocyanins has been proposed based on a comparison of the two *Limulus* II structures with the previously determined structure of *P. interruptus* hemocyanin (Hazes *et al*., 1993; Magnus *et al*., 1994). The key element in this model is a rotation of domain 1 with respect to domains 2 and 3. This couples the changes at the oxygen-binding site to the allosteric transition between the R and T-states, see Figure 1. The trigger for the domain 1 rotation is a decrease in Cu-Cu distance from 4.6 Å, as observed in deoxygenated *Limulus* II hemocyanin, to 3.6 Å as observed in oxygenated *Limulus* II hemocyanin. The movement of the copper ions would then be passed on to the first domain by the close interaction between the imidazole of the copper ligand His328 in the second domain and the aromatic ring of Phe49 in the first domain, see Figure 1(b). The proposed rotation of domain 1, away from domain 2, is actually observed in the *Panulirus* structure. The model also explains the strong allosteric effect of chloride ions, since the chloride ion is bridging the domain 1-domain 2 interface, with one protein side-chain of each domain coordinating the chloride ion, see Figure 1(b).

In an attempt to obtain the *Limulus* II structure in the R-state, we have grown crystals in the absence of NaCl (these will be referred to as low-salt crystals in contrast to the high-salt crystals used in previous studies). We added $Ca(NO_3)_2$, since Ca^{2+} has been reported to stabilize the *Limulus* II hexameric structure (Brenowitz *et al*., 1984). In addition, we added minute amounts of $HgCl_2$, since mercury was reported to stabilize the R-state conformation of the native hemocyanin complex (Brouwer *et al*., 1983). We describe here the 2.4 Å crystal structure of oxygenated *Limulus* II hemocyanin grown in the presence of $Ca(NO_3)_2$, and $HgCl_2$, and discuss the potential implications of this structure for the allosteric regulation of *L. polyphemus* hemocyanin under physiological conditions.

Results

Quality of the structure

The final model for the low-salt structure contains 4933 protein atoms in 607 residues, two copper ions, one calcium ion, one nitrate ion, one dioxygen molecule and 212 water molecules. The *R*-value for all reflections between 2.4 and 8 Å is 18.1% and the deviations from ideal bond lengths and bond angles are 0.018 Å and 3.4°, respectively. The coordinate error estimate, as given by the program SIGMAA, is 0.22 Å (Read, 1986). The second domain, comprising residues 151 to 380, has relatively low *B*-values (11.3 $Å^2$ on average), which is also reflected in the clear density for this part of the model. The first and third domains, residues 1 to 150 and 381 to 628, respectively, have higher average *B*-values (22.0 $Å^2$ for domain 1 and 17.5 $Å^2$ for domain 3). In these domains, four regions of the polypeptide chain, comprising a total of 21 residues, had uninterpretable density and hence are not included in the model. These stretches include residues 22 to 29, 134 to 138, 527 to 530 and 569 to 572. In addition, the side-chains of residues Asp146, Asn152, Leu505, Lys550 and Ser573 could not be built unambiguously, and atoms beyond C^{β} have not been included in the model. In the previously described high-salt deoxygenated structure (Hazes *et al*., 1993) the same 21 residues plus an additional seven residues (residues 1, 21, 132, 133, 139, 148 and 149) could also not be interpreted.

Analysis of the protein geometry with the program PROCHECK (Laskowski *et al*., 1993) indicated that the geometry of our model is better than expected for a 2.4 Å structure on all properties evaluated by the program. The ϕ, ψ plot (Ramakrishnan & Ramachandran, 1965) produced by PROCHECK is given in Figure 2.

Structural comparisons

A comparison of the two high-salt structures with the low-salt structure shows that all 600 C^{α}-atoms of the deoxygenated high-salt structure can be superimposed on the oxygenated low-salt structure with a root-mean-square (rms) deviation

of 0.21 Å. For the oxygenated high-salt structure, 567 C^{α}-atoms, out of the 573 residues in the model, can be superimposed with an rms deviation of 0.26 Å. In view of the lower completeness of the oxygenated high-salt model, and the fact that the main-chain conformation of the two high-salt structures are virtually identical, we will carry out all further comparisons with the deoxygenated high-salt structure. When all non-hydrogen atoms are considered, 4842 equivalent atoms can be superimposed with an rms deviation of 0.40 Å and, when leaving out the 76 atoms that deviate by more than 5σ, this value is reduced to 0.29 Å. No significant rotation or translation was required to superimpose the low-salt and high-salt structures, indicating that also the hexameric quaternary structures have remained unchanged. Comparison of the relative positions of the three domains with respect to each other showed that the packing of the first and second domains in the high-salt and low-salt structures is virtually identical, whereas the relative position of domain three differs by a rotation of only 0.4° and a translation of 0.1 Å.

The 76 atoms that were rejected from the superposition at a 5σ level are contained in 40 residues, most of which are hydrophilic and exposed to the solvent. No obvious reason for the different side-chain conformations could be found with the exception of two residues. One is the copper ligand His364, which changes its confor-

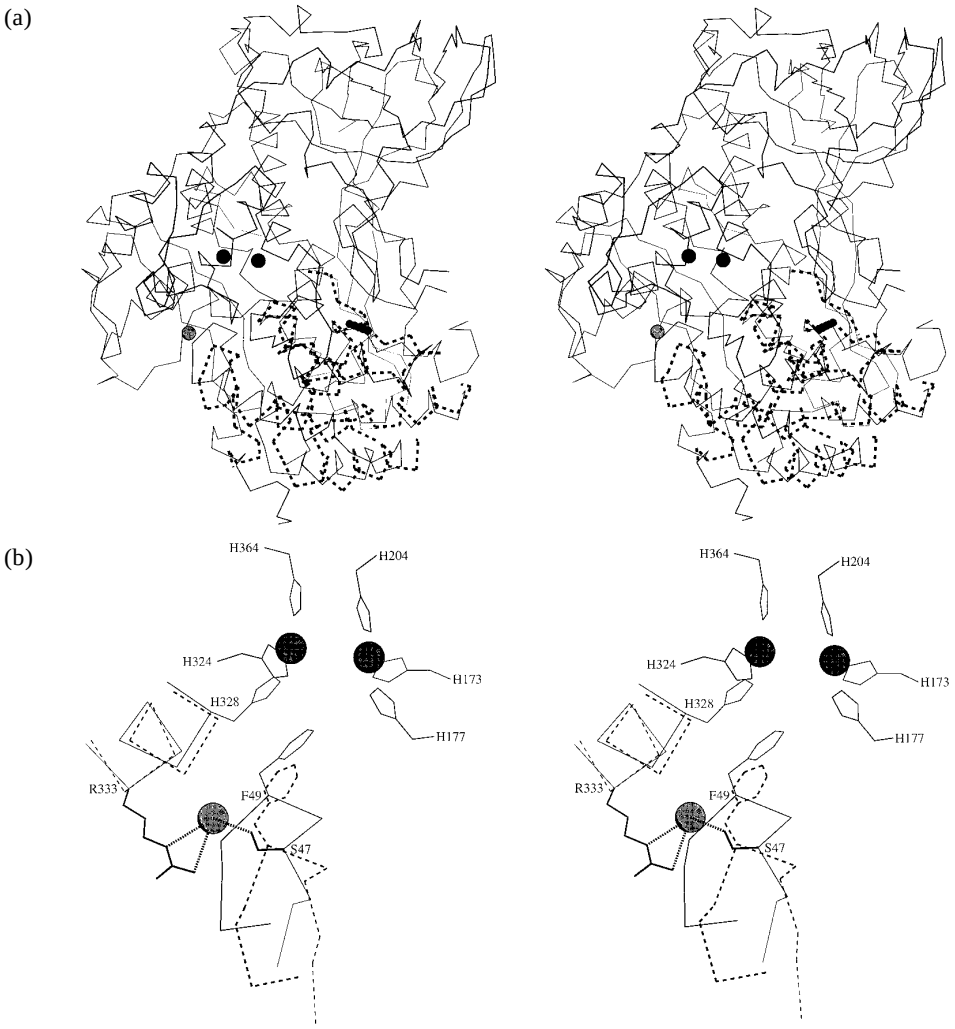

Figure 1. Stereo diagram of the domain 1 rotation and its proposed consequences for allosteric regulation. (a) The C^{α} trace of the full *Limulus* II subunit is shown plus the copper ions (black spheres), the chloride ion (grey sphere), and the domain 1 rotation axis (represented by a row of five spheres at a 10 Å interval). The domain 1 rotation axis is oriented perpendicular to the plane of the paper. The first domain of the *Panulirus* structure is shown in broken lines. For clarity, only the regions of domain 1 that have a structural homologue in the *Limulus* II structure are shown. The position for domain 1 of the *Panulirus* structure was obtained after superpositioning the second domains of both hemocyanins. This illustrates the 7.5° rotation of domain 1 relative to domain 2. (b) Enlarged stereodiagram of the oxygen and chloride-binding sites in the same orientation as (a). Residues are labelled with their one-character amino acid code followed by the residue number of the *Limulus* II structure. Movement of the domain l loop releases the tight packing of the Phe49 and His328 side-chains in the *Limulus* II structure and at the same time it displaces the chloride ligand Ser47. This Figure was created with the MOLSCRIPT program (Kraulis, 1991).

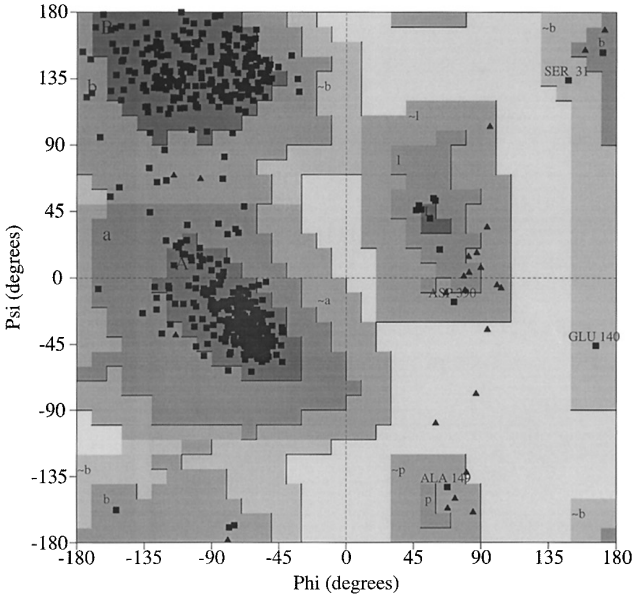

Figure 2. The ϕ, ψ plot of the final model generated by the PROCHECK program (Laskowski *et al*., 1993). Four regions are distinguished by a varying grey-scale. These represent, in order of increasing darkness, disallowed regions, generously allowed regions, additional allowed regions and most favoured regions. The percentage of residues in each region is; 0.0, 0.8, 9.2 and 90.1, respectively.

mation in response to the decrease of the Cu-Cu distance from 4.6 Å in the deoxygenated structure to 3.6 Å in the oxygenated structure. This change involves the imidazole ring of this residue, which rotates by 11° about the torsion angle χ1 and by 163° about χ2 in order to maintain a proper coordination of the copper ion. The His364 conformation in the oxygenated low-salt structure is indeed very similar to the conformation observed in the oxygenated high-salt structure and the deoxygenated *P. interruptus* structure, all of which have a short Cu-Cu distance in common. Overall, the stereochemistry of the dinuclear copper site in the oxygenated low-salt structure is very similar to what was found for the oxygenated high-salt structure (Magnus *et al*., 1994) and it is therefore not presented here in detail.

The second residue that showed a potentially significant side-chain reorientation is Met223. In the high-salt structures the side-chain is in a buried position, whereas in the low-salt structure the side-chain is rotated outward into the solvent. Some weak density was still present in the cavity formed by the withdrawal of the Met223 side-chain. Interestingly, the cavity contains the sulphydryl group of Cys208 and might therefore represent a mercury-binding pocket. However, the strength of the density and the 4.3 Å distance from the Cys208 sulphur atom argue against the presence of a mercury ion. Instead, the density could be modelled as a water molecule, which refined to a *B*-value of 15 Å^2. On the basis of the electron density map no mercury ion could be detected at this or any other site in the protein. Accordingly, the mercury concentration in the dialysis buffer or the duration of the dialysis must have been insufficient to allow the mercury sites to become significantly occupied. Alternatively, the mercury-binding sites that were reported for the native 48-meric *Limulus* hemocyanin complex (Brouwer *et al*., 1983) may not exist in the *Limulus* II subunit.

Nitrate binding

During the refinement a strong feature was observed in the electron density map at the chloride-binding site. This density had a somewhat flattened trigonal shape, see Figure 3(a), unlike the spherical density that was observed for the chloride ion in the high-salt structures. Inclusion of a chloride ion in the model indeed could not fit the density satisfactorily, and three additional density features showed up in the $F_o - F_c$ map just around the chloride ion. The same three density features were seen in a difference map based on the low-salt oxygenated crystal amplitudes minus the high-salt deoxygenated crystal amplitudes, using the phases of the high-salt structure, see Figure 3(b). Based on the shape of the density, a small trigonal planar compound had to be present. Among the compounds available in the crystallization medium, nitrate is the only suitable candidate, since the reservoir solution contained approximately 60 mM nitrate. A nitrate ion could indeed be fitted nicely in the density and after refinement no significant peak was left in the $F_o - F_c$ map at this position. In the final model, the *B*-values of the nitrate atoms had refined to 16.9, 16.5, 15.3 and 16.5 Å^2 for the nitrogen atom and the three oxygen atoms, respectively. This is quite similar to the *B*-value of 18.9 Å^2 that was observed for the chloride ion in the deoxygenated high-salt structure.

The nitrate ion is coordinated by the same protein ligands, Ser47 and Arg333, as the chloride ion in the high-salt structures. The positive charge of Arg333 interacts favourably with the negative charge of nitrate and hydrogen bonds are formed between two nitrate oxygen atoms and the Arg333 N^{ϵ} and N^{η} atoms. The third nitrate oxygen atom forms a hydrogen bond to the side-chain hydroxyl of Ser47. See Table 1 and Figure 4(a).

Calcium binding

In the high-salt structure, a metal-binding site was observed in the third domain of the protein (Hazes *et al*., 1993). In view of the reported functional and structural interactions of *Limulus* II hemocyanin with calcium ions (Brenowitz *et al*., 1984; Brouwer *et al*., 1983) it was suggested that this site might represent a calcium-binding site. The octahedral coordination by six oxygen atoms including a negatively charged aspartate side-chain oxygen atom is indeed consistent with such a binding site (Strynadka & James, 1989). However,

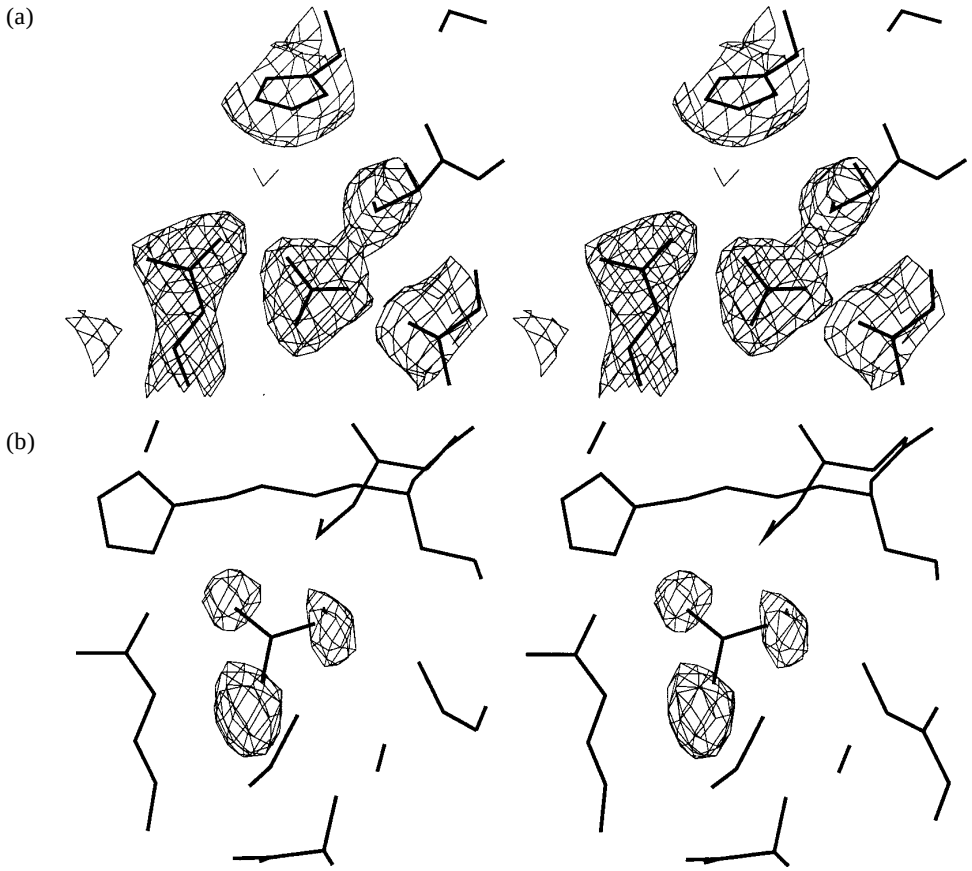

Figure 3. (a) The $2F_o - F_c$ electron density map around the nitrate ion contoured at a 1σ level. A model for nitrate has been included in the Figure for illustration purposes only. It was not present in the model from which the structure factors were calculated. (b) Difference map based on the low-salt oxygenated crystal amplitudes minus the high-salt deoxygenated crystal amplitudes and using the phase information from the high-salt deoxygenated structure. Contours are at a 3σ level. The resulting map gives density peaks at positions where more scattering matter is present in the low-salt crystal than in the high-salt crystal. This clearly reveals the nitrate oxygen atoms. No density is present for the central nitrogen atom, since it is cancelled out by the chloride ion that is present in the high-salt crystal.

since the high-salt crystals were grown in the presence of EDTA and high concentrations of NaCl, a sodium ion was believed to occupy this site in the crystal structure instead of calcium. In contrast, the low-salt crystals were grown from a solution containing approximately 25 mM free Ca^{2+} and a low sodium concentration. Consequently, the metal bound to the low-salt structure is most likely a calcium ion. Additional evidence for this assignment comes from a difference map based on the low-salt oxygenated crystal amplitudes minus the high-salt deoxygenated crystal amplitudes using phases derived from the high-salt model (not shown). This map showed a peak at the metal-binding site, which supports the notion that in the low-salt crystals a stronger scatterer is present than in the high-salt crystals. In the final low-salt structure the *B*-value of the calcium ion refined to

Table 1. Hydrogen-bond geometry of the nitrate ion

Distances (Å)				Angles (deg.)[a]	
O-1–Arg N^{ϵ}	2.9	N–O-1–Arg N^{ϵ}	104	Arg C^{ζ}–Arg N^{ϵ}-O-1	118
O-2–Ser O^{γ}	2.6	N–O-2–Ser O^{γ}	79	Ser C^{β}–Ser O^{γ}–O-2	98
O-3–Ser O^{γ}[b]	3.2	N–O-3–Ser O^{γ}	112	Ser C^{β}–Ser O^{γ}–O-3	78
O-3–Arg N^{ϵ}	3.1	N–O-3–Arg N^{ϵ}	96	Arg C^{ζ}–Arg N^{ϵ}–O-3	79
O-3–Arg N^{η}	2.5	N–O-3–Arg N^{η}	132	Arg C^{ζ}–Arg N^{η}–O-3	104

During refinement none of the distances or angles was restrained. The location of the oxygen atoms O-1, O-2 and O-3 is depicted in Figure 4(a).

[a] The planes of the nitrate and guadinium group make an angle of 38°.

[b] Nitrate oxygen atoms O-2 and O-3 are both within hydrogen-bonding distance of the side-chain oxygen atom of Ser47. Since the serine hydroxyl group can provide only one proton, the less favourable hydrogen bond to O-3 probably plays no significant role in the binding of nitrate.

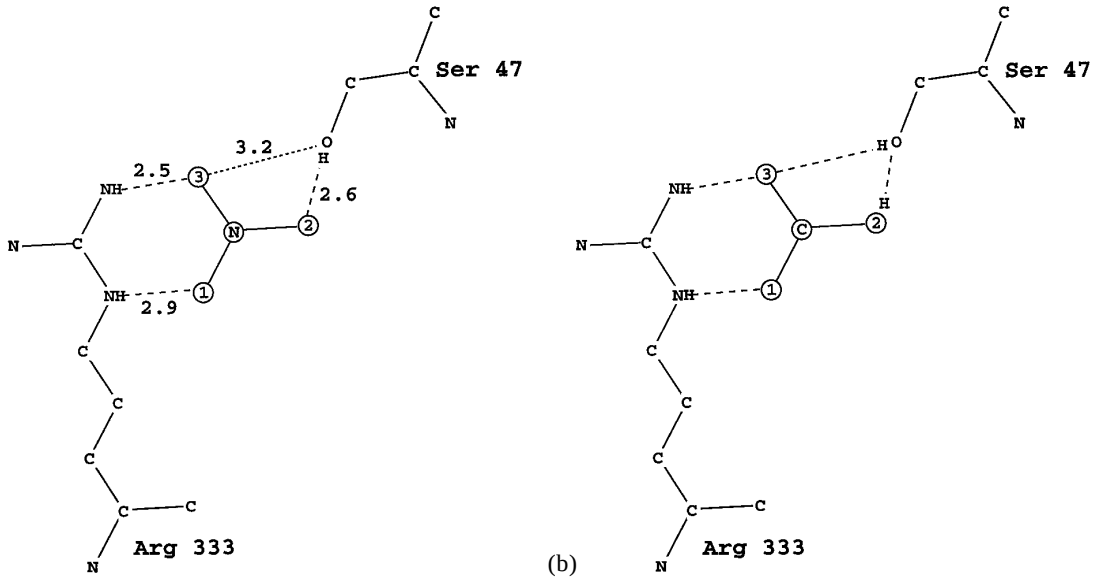

Figure 4. (a) A diagram showing the hydrogen bonds between nitrate and the protein ligands Arg333 and Ser47. Only the hydrogen atoms involved in hydrogen bonds are indicated, and the nitrate oxygen atoms are labelled in accordance to the numbering scheme used in Table 1. The dotted line between Ser47 and nitrate O-3 indicates that both atoms are just within hydrogen-bonding distance. However, the hydroxyl proton of Ser47 is already engaged in a shorter hydrogen bond to nitrate O-2. Accordingly, the interaction with O-3 does not seem to play a significant role in the binding of nitrate. (b) A diagram showing the putative binding geometry of bicarbonate. In addition to the interactions made by nitrate, bicarbonate can make the hydrogen bond between Ser47 and O-3 using its own hydrogen atom. In principle, both the O-2 and O-3 bicarbonate oxygen atoms can act as a hydrogen bond donor, and an equilibrium between both situations most likely exists. However, the situation where O-2 acts as the donor, as depicted, appears to yield a more favourable charge interaction between bicarbonate and Arg333.

22 Å^2. The coordination geometry of the calcium ion in the low-salt structure and the sodium ion in the high-salt structure are very similar, though most coordination distances to the calcium ion are slightly smaller, see Table 2.

Oxygen-binding studies

Oxygen-binding experiments were carried out to establish if the observed nitrate binding has functional consequences for *Limulus* II hemocyanin at the concentrations employed during crystallisation. Figure 5 shows the oxygen affinity for purified *Limulus* II hemocyanin as a function of chloride and nitrate concentrations, see the legend for details. Hill coefficients that were derived from six measurements between 30% and 70% oxygen saturation did not deviate significantly from 1.0, indicating that the protein is not cooperative under these conditions.

Table 2. Coordination distances of the calcium ion in the low-salt structure and the sodium ion in the high-salt structure

	Ca^{2+} (Å)[a]	Na^{+} (Å)[b]
Ser507 O	2.2	2.3
Thr510 O	2.4	2.4
Asp578 O	2.1	2.3
Asp578 O^{δ}	2.5	2.8
Wat1	1.8	2.4
Wat2	2.5	3.0

[a] This work.
[b] Values taken from Hazes *et al*. (1993).

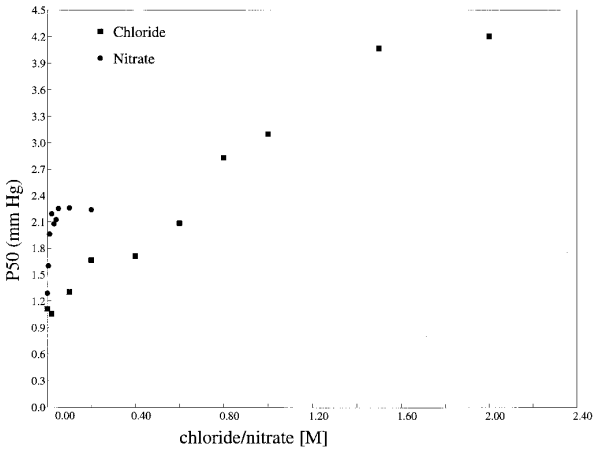

Figure 5. Oxygen-binding curves for *Limulus* II hemocyanin as function of chloride and nitrate concentration. Measurements were made by the tonometric method (Riggs & Wolbach, 1956) at 20°C in 5 mM Hepes buffer (pH 7.5), 10 mM EDTA. The salt concentrations were raised by adding small amounts of either 5 M NaCl or 2 M $NaNO_3$ stock solutions to 1.5 ml of a 3 mg/ml solution of purified *Limulus* II hemocyanin.

Discussion

Conformational state of the low-salt structure

The low-salt and high-salt structures of *Limulus* II hemocyanin show no significant difference in their tertiary and quaternary structures. Within the framework of the postulated allosteric regulation mechanism, the high-salt *Limulus* II structures represent T-state conformations (Hazes *et al*., 1993). Hence, the low-salt structure reported here should also be considered to represent a T-state conformation. As previously noted, oxygen-binding studies indicate that the existence of the unusual oxygenated T-state structure in the high-salt crystals is most likely caused by the 0.5 M NaCl present in the crystallization buffer. In structural terms this means that the binding of chloride in the domain 1-domain 2 interface prevents the allosteric T to R-state transition for the *Limulus* II hexamer. Accordingly, the observation of an oxygenated T-state in the low-salt structure suggests that 60 mM nitrate has a similar effect on the *Limulus* II hexamer. Our oxygen-binding data indeed indicate that nitrate, like chloride, reduces the oxygen affinity (Figure 5). Furthermore, the nitrate effect saturates at approximately 20 mM concentrations in contrast to the chloride effect, which levels off only at concentrations above 1.5 M. It should be noted that at the pH of 7.5 and in presence of EDTA, the *Limulus* II preparation is expected to be in a monomeric state for the nitrate-binding measurements and the low ionic-strength chloride measurements. This agrees with the observed Hill coefficients of 1.0. At chloride concentrations of 0.5 M and higher hexamerization of *Limulus* II is induced (Brenowitz *et al*., 1984). This could cause a further depression of the oxygen affinity, which may at least partly explain the stronger reduction of the oxygen affinity by chloride at high concentrations. (The Hill coefficient of *Limulus* II hexamers at high chloride concentration is still 1.0, since the chloride ions fix the hexamer in a non-cooperative low-affinity state. Weakly cooperative *Limulus* II hexamers can be obtained when hexamerization is induced by calcium (Brenowitz *et al*., 1984).)

Physiological importance of nitrate and bicarbonate

Nitrate is not a normal component of hemolymph and it is therefore unlikely that nitrate itself plays a physiological role as an allosteric regulator. However, the observation that two relatively dissimilar anions can bind to the same site with comparable functional consequences suggests that there might be other small anions that can functionally substitute for the chloride ion. Interestingly, the existence of a rather unspecific binding site for small anions on *L. polyphemus* hemocyanin has been proposed previously based on oxygen-binding studies (Brouwer *et al*., 1977). In that study binding of the anion was also linked to a reduction in oxygen affinity, suggesting that their anion-binding site and the chloride-binding site might be identical.

As detailed above, it appears that various anions can function as allosteric effectors by binding at the site that was first designated in *Limulus* II as the chloride-binding site. A particularly interesting compound in this respect is bicarbonate. Bicarbonate is a close structural analogue of nitrate and molecular modelling suggests that it can bind in a similar fashion, see Figure 4(b). The existence of an allosteric binding site for bicarbonate would allow this metabolic by-product to have a direct impact on oxygen uptake and delivery. Intriguing combinations of effects can be considered, since bicarbonate would compete with chloride for the same binding site and it can interact with protons and divalent cations, both of which are themselves allosteric effectors.

An effect of bicarbonate on the oxygen affinity of *L. polyphemus* hemocyanin has been reported (Mangum & Burnett, 1986) but, contrary to our expectation, the oxygen affinity increased. However, bicarbonate also interacts with divalent cations, especially through the unprotonated carbonate species, and Mangum & Burnett (1986) pointed out that, since calcium is an allosteric effector that lowers oxygen affinity, the interaction between calcium and carbonate would raise the oxygen affinity. They showed that this indirect effect could indeed explain the bicarbonate-induced increase in oxygen affinity in their experiments. Clearly, the net effect of bicarbonate will depend on the relative strength of the calcium-mediated effect and the postulated protein-mediated effect. The former will be enhanced at elevated pH, which promotes carbonate formation, whereas the latter will be enhanced at low salinity, since bicarbonate would have to compete with chloride for the same site. In this respect it is interesting to note that the experiments by Mangum & Burnett (1986) were conducted at a pH of 8.2 in a high salinity saline. This saline represents the upper limit of the physiological hemolymph salinity and is thus least favourable to observe the postulated bicarbonate effect. In addition, the pH of 8.2 exceeds the physiological pH, which is normally 7.5 but can be as low as 7.0 (Johansen & Petersen, 1975), but the impact of this on the calcium-mediated effect is probably small.

During the life-cycle of *L. polyphemus* the organism encounters various external conditions that affect its respiration. In the spring it migrates into low-salinity estuaries where its hemolymph chloride concentration can drop twofold, resulting in a significant increase in hemocyanin oxygen affinity. In a hypoxic environment the hemolymph pH is reduced which, due to the reversed Bohr effect, also leads to an increased oxygen affinity. Air exposure has also been regarded as a hypoxic condition and, likewise, a reduction in hemolymph

pH has been reported (Johansen & Petersen, 1975; Towle *et al*., 1982; Mangum, 1983). All three conditions mentioned above lead to an increase in hemocyanin oxygen affinity, which is the proper adaptation to hypoxic conditions. However, it is conceivable that there are situations where the reversed Bohr and/or chloride effects yield an oxygen affinity that is too high for the given external oxygen pressure. The reduction of hemolymph chloride concentrations in dilute waters is of special interest, since at the lower chloride concentrations, the proposed bicarbonate effect is expected to become more significant. In addition, dilute waters are not necessarily hypoxic and in that case the increased oxygen affinity would be maladaptive. Mangum *et al*. (1976) have shown that bradycardia is employed to maintain the oxygen carrying capacity of *L. polyphemus* hemocyanin under low-salt conditions. However, this also represents a situation where bicarbonate might contribute to stimulate oxygen release in the tissues. Unfortunately, most studies that investigate the effect of the environment on hemolymph composition have focused on hypoxic conditions or air-exposed animals (Johansen & Petersen, 1975; Towle *et al*., 1982). Towle *et al*. (1982) and Mangum *et al*. (1976) also present data on the effect of changes in salinity under normoxic conditions. They report that the change in salinity does not significantly affect the hemolymph pH, whereas the bicarbonate concentration is higher in animals that are adapted to low-salinity conditions, 2.58($\pm$0.52) mM and 3.91($\pm$0.62) mM, respectively (Towle *et al*., 1982). As explained above, the higher oxygen affinity in low salinity is unfavourable under normoxic conditions. The observed increase in hemolymph bicarbonate concentration may therefore function to compensate for the lack of chloride, but far more data will be required to support such a conclusion.

Concluding remarks

The current model for allosteric regulation in arthropodan hemocyanins assumes that the first domain rotates away from the second domain in the allosteric transition from the T to the R-state (Hazes *et al*., 1993; Magnus *et al*., 1994). Chloride binding to a site in the domain 1-domain 2 interface of *Limulus* II hemocyanin stabilizes the T-state and therefore lowers the oxygen affinity. Here, we report that nitrate binds to the same site as chloride and oxygen-binding data indeed show that nitrate reduces the oxygen affinity of *Limulus* II hemocyanin. This finding suggests that the chloride-binding site is actually a more general binding site for small anions, possibly identical with the anion-binding site that was previously proposed based on oxygen-binding studies (Brouwer *et al*., 1977). Molecular modelling predicts that bicarbonate can bind at this site as well, and we have high-lighted a potential effect of bicarbonate on oxygen affinity, since bicarbonate is closely related to metabolic activity. We have proposed an adaptive importance of the proposed bicarbonate effect in a low-salinity environment. However, it is still premature to discuss potential adaptive strategies in any detail. The first step clearly has to be to establish whether the proposed bicarbonate effect can be demonstrated under physiological conditions. Experiments are being performed by one of the authors (C.B.) to demonstrate such an effect and its dependence on pH, divalent cations and chloride ions.

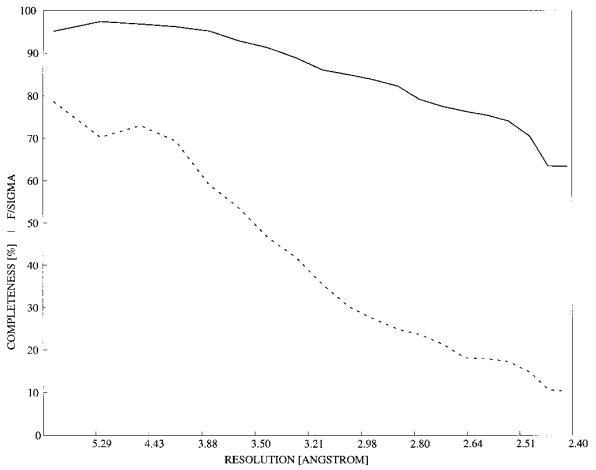

Figure 6. Plot of the percentage completeness (continuous line) and the $F/\sigma F$ ratio (broken line) of the data set. (The scale on the *y*-axis is valid for both curves.) The total number of reflections is 24,861, which corresponds to the expected number of reflections for a 100% complete data set to 2.56 Å. The statistics for this Figure were produced by the program SFTOOLS (B.H., unpublished).

Materials and Methods

Crystallization and data collection

Purified *Limulus* II hemocyanin was prepared as described (Brenowitz *et al*., 1981). A 100-µl sample of protein material at 40 mg/ml was dialysed overnight against 50 ml of a solution containing 50 mM glycine, 50 mM Tris-HNO_3 (pH 8.9) to which 50 µl of a solution containing 2 mg $HgCl_2$/ml was added. This results in a Hg^{2+} concentration of $\sim$7 µM in the dialysis solution and a stoichiometry of approximately six mercury ions per *Limulus* II subunit. Excess mercury was removed the next day by a second dialysis against 50 ml of a buffer containing 50 mM glycine, 50 mM Tris-HCl (pH 8.9), 10 mM EDTA. *L. polyphemus* hemocyanin has been reported to contain three non-EDTA-removable mercury-binding sites per subunit (Brouwer *et al*., 1983). The resulting protein solution (25 mg/ml) was used for crystallization at room temperature by the hanging drop method (McPherson, 1990). Drops were formed from 5 µl of protein solution and 5 µl of reservoir solution and equilibrated over wells with 630 µl of reservoir solution. The reservoir solution was prepared by mixing: (1) 40 µl of a buffer containing 0.5 M glycine, 0.1 M EDTA, 0.5 M Tris-HNO_3, pH 8.9; (2) 110 µl of 1 M bisTris, pH 6.0; (3) 200 µl of 0.1 M $Ca(NO_3)_2$; (4) 10 µl of a solution made

by adding 10 ml of doubly distilled water to 5 g of PEG 6000; and (5) 270 µl of doubly distilled water.

From a single crystal grown under these conditions a data set was collected at room temperature on an Enraf-Nonius FAST area-detector employing CuKα radiation from an Elliot GX-21 rotating anode. Data were processed by the program MADNES (Pflugrath & Messerschmidt, 1986) using the profile fitting procedure (Kabsch, 1988). In all, 124,135 observations from three crystal settings were scaled and merged by the programs SCALKB2 and KBAPLY from the BIOMOL software package (University of Groningen). In total, 24,861 unique reflections to a resolution of 2.41 Å were obtained, giving an overall completeness of 83:7% (78.0% > 3σ) with an R_{sym} of 5.2% ($R_{sym} = 100\Sigma|I - \langle I \rangle| / \Sigma I$). The completeness and the $F/\mathrm{Sig}F$ ratio as function of resolution is given in Figure 6.

Refinement

The space group and cell parameters of the low-salt crystals are identical with those of the high-salt crystals (space group *R*32, rhombohedral setting: $a = b = c =$ 117.0 Å, $\alpha = \beta = \gamma = 60.0°$). Refinement was therefore started directly from the deoxygenated high-salt *Limulus* II structure. The side-chains of the copper ligands (His residues 173, 177, 204, 324, 328 and 364), the chloride ligands (Ser47 and Arg333), the sodium ligand (Asp578) and the ''allosteric sensor'' Phe49 were removed from the model to assure an unbiased density for these important residues. Also, both copper ions, the chloride ion, the sodium ion and all water molecules were left out of the initial model. Refinement was performed with the program XPLOR (Brünger *et al*., 1987), using all data between 2.4 and 8.0 Å.

In the first refinement cycle, residues 2 to 131 (domain 1), residues 140 to 147 (the domain 1-domain 2 linker) and residues 150 to 628 (domains 2 and 3) were treated as rigid bodies. This refinement reduced the initial *R*-factor only from 27.8 to 27.2%, and no significant rigid body movements were observed. In the next step the *B*-values, which were taken from the high-salt structure, were replaced by an overall *B*-value of 20.0 Å^2 and subsequently refined to a final overall *B*-value of 13.2 Å^2. The *R*-value for this structure was 30.9%. One energy minimization run lowered the *R*-value to 25.9%. In the resulting $F_o - F_c$ map, strong signals for the copper ions (at 16.6 and 15.2σ, respectively) and a calcium ion were observed. There was density present at the chloride-binding site.

During the subsequent model-building session, using the program FRODO (Jones, 1978), all side-chains that were left out of the model showed clear density and hence were reincorporated into the model. Also, the copper ions and a calcium ion were reintroduced with a charge of zero and a van der Waals radius of 0.15 Å. The zero-charge and small van der Waals radius were given to obtain positions for these ions that are essentially based only on the observed structure factors. Energy minimization of this model was followed by a *B*-value refinement allowing overall *B*-values for the three domains (residues 2 to 150, 151 to 380 and 381 to 628). This resulted in an *R*-value of 24.1%. In the $F_o - F_c$ map calculated from this model, strong density was again observed at the chloride-binding site. Although the density did not have a spherical shape, a chloride ion was included at this stage. Also, a dioxygen molecule could be fitted between both copper ions. The bond between the dioxygen atoms, which is bound as a peroxide (Thamann *et al*., 1977), was restrained to 1.41 Å. This is the observed bond length in a synthetic analogue of the dinuclear copper center of hemocyanins (Kitajima *et al*., 1989, 1992). Again, the chloride ion and the dioxygen atoms were given a charge of zero and a van der Waals radius of 0.15 Å. In addition, 177 water molecules were positioned at peaks in the $F_o - F_c$ map, with each water molecule making at least one hydrogen bond with the protein.

Subsequent energy minimization lowered the *R*-value of the model to 21.6%. In the $F_o - F_c$ map from this model three additional density features showed up around the chloride ion. Since nitrate, which was present in the crystallization medium whereas chloride was not, fitted beautifully in this density, the chloride ion was replaced by a nitrate ion with its atomic charges set to zero. The bond lengths and bond angles in the nitrate ion were restrained to 1.24 Å and 120°, respectively, and the van der Waals radii of the nitrate atoms were again set to 0.15 Å. In the same session, the number of water molecules was increased to 212. During the previous refinement cycle the oxygen molecule, which had been inserted symmetrically between the two copper ions, had shifted towards the Cu-A ion. This resulted in unrealistically short coordination distances with Cu-A (<1.8 Å) and rather long coordination distances with Cu-B (>2.0 Å). The position of the oxygen molecule in between two strong scatterers, the copper ions, renders it very sensitive to small errors in the positions or *B*-values of the copper ions. The observed deviations from a symmetric binding mode are therefore most likely artifacts, and in the next refinement cycle the Cu-oxygen distances were weakly restrained to 1.91 Å (a bonded restraint of 250.0 in parameter set param19x.pro was given). In a last energy minimization run, the *R*-value of the model dropped to 20.0%. A subsequent restrained *B*-value refinement yielded the final structure with an *R*-value of 18.1%. *B*-value restraints used were 0.5 Å^2 for bonded main-chain atoms and 1.0 Å^2 for main-chain atoms related by a bond angle. For side-chain atoms, these values were 1.0 and 2.0 Å^2, respectively.

The coordinates have been deposited at the Brookhaven Protein Data Bank with accession code 1NOL.

Acknowledgements

This research was supported by the Netherlands Foundation for Chemical Research (SON) with financial aid from the Netherlands Organization for Scientific Research (NWO). K.A.M. and C.B. gratefully acknowledge support from the U.S. National Science Foundation (grant MCB 9305250). The authors thank Shirly Tesh for performing the oxygen-binding measurements.

References

Brenowitz, M., Bonaventura, C., Bonaventura, J. & Gianazza, E. (1981). Subunit composition of a high molecular weight oligomer: *Limulus polyphemus* hemocyanin. *Arch. Biochem. Biophys.* **210**, 748–761.

Brenowitz, M., Bonaventura, C. & Bonaventura, J. (1984). Self-association and oxygen-binding characteristics of the isolated subunits of *Limulus polyphemus* hemocyanin. *Arch. Biochem. Biophys.* **230**, 238–249.

Brouwer, M. & Serigstad, B. (1989). Allosteric control in *Limulus polyphemus* hemocyanin: functional rel-

evance of interactions between hexamers. *Biochemistry*, **28**, 8819–8827.

Brouwer, M., Bonaventura, C. & Bonaventura, J. (1977). Oxygen binding by *Limulus polyphemus* hemocyanin: allosteric modulation by chloride ions. *Biochemistry*, **16**, 3897–3902.

Brouwer, M., Bonaventura, C. & Bonaventura, J. (1982). Chloride and pH dependence of cooperative interactions in *Limulus polyphemus* hemocyanin. In *Physiology and Biology of Horseshoe Crabs: Studies on Normal and Environmentally Stressed Animals* (Bonaventura, J., Bonaventura, C. & Tesh, S., eds), pp. 231–256, Alan R. Liss, Inc. New York.

Brouwer, M., Bonaventura, C. & Bonaventura, J. (1983). Metal ion interactions with *Limulus polyphemus* and *Callinectes sapidus* hemocyanins: stoichiometry and structural and functional consequences of calcium(II), cadmium(II), Zinc(II), and mercury(II) binding. *Biochemistry*, **22**, 4713–4723.

Brünger, A. T., Kuriyan, J. & Karplus, M. (1987). Crystallographic *R*-factor refinement by molecular dynamics. *Science*, **235**, 458–460.

Drexel, R., Siegmund, S., Schneider, H.-J., Linzen, B., Gielens, C., Préaux, G., Lontie, R., Kellermann, J. & Lottspeich, F. (1987). Complete amino-acid sequence of a functional unit from a molluscan hemocyanin (*Helix pomatia*). *Biol. Chem. Hoppe-Seyler*, **368**, 617–635.

Ellerton, H. D., Ellerton, N. F. & Robinson, H. A. (1983). Hemocyanin—a current perspective. *Prog. Biophys. Mol. Biol* **41**, 143–248.

Gaykema, W. P. J., Hol, W. G. J., Vereijken, J. M., Soeter, N. M., Bak, H. J. & Beintema, J. J. (1984). 3.2 Å structure of the copper-containing, oxygen-carring protein *Panulirus interruptus* haemocyanin. *Nature*, **309**, 23–29.

Hazes, B., Magnus, K. A., Bonaventura, C., Bonaventura, J., Dauter, Z., Kalk, K. H. & Hol, W. G. J. (1993). Crystal structure of deoxygenated *Limulus polyphemus* subunit II hemocyanin at 2.18 Å resolution: clues for a mechanism for allosteric regulation. *Protein Sci.* **2**, 597–619.

Johansen, K. & Petersen, J. A. (1975). Respiratory adaptations in *Limulus polyphemus* (L.). In *Physiological Ecology of Estuarine Organisms* (Vernberg, F. J., ed.), pp. 129–145, University of South Carolina Press, Columbia, SC.

Jones, T. A. (1978). A graphics model building and refinement system for macromolecules. *J. Appl. Crystallog.* **11**, 268–272.

Kabsch, W. (1988). Evaluation of single-crystal X-ray diffraction data from a position-sensitive detector. *J. Appl. Crystallog.* **21**, 916–924.

Kitajima, N., Fujisawa, K. & Moro-oka, Y. (1989). μ-η^2:η^2-Peroxo binuclear copper complex, $[Cu(HB(3,5\text{-}iPr_21Pz)_3)]_2(O_2)$. *J. Am. Chem. Soc.* **111**, 8975–8976.

Kitajima, N., Fujisawa, K., Fujimoto, C., Moro-oka, Y., Hashimoto, S., Kitagawa, T., Toriumi, K., Tatsumi, K. & Nakamura, A. (1992). A new model for dioxygen binding in hemocyanin. Synthesis, characterisation, and molecular structure for the μ-η^2:η^2 Peroxo dinuclear copper(II) complexes, $[Cu(HB(3,5\text{-}R_2Pz)_3)]_2(O_2)$ (R = *i*-pr and Ph). *J. Am. Chem. Soc.* **114**, 1277–1291.

Kraulis, P. (1991). MOLSCRIPT: a program to produce both detailed and schematic plots of protein structures. *J. Appl. Crystallog.* **24**, 946–950.

Lamy, J., Lamy, J., Sizaret, P.-Y., Billiald, P., Jollès, P., Jollès, J., Feldmann, R. J. & Bonaventura, J. (1983). Quaternary structure of *Limulus polyphemus* hemocyanin. *Biochemistry*, **22**, 5573–5583.

Lang, W. H. & Van Holde, K. E. (1991). Cloning and sequencing of *Octopus dofleini* hemocyanin cDNA: derived sequences of functional units Ode and Odf. *Proc. Natl. Acad. Sci. USA*, **88**, 244–248.

Laskowski, R. A., MacArthur, M. W., Moss, D. S. & Thornton, J. M. (1993). PROCHECK: a program to check the stereochemical quality of protein structures. *J. Appl. Crystallog.* **26**, 283–291.

Magnus, K. A., Hazes, B., Ton-That, H., Bonaventura, C., Bonaventura, J. & Hol, W. G. J. (1994). Crystallographic analysis of oxygenated and deoxygenated states of arthropod hemocyanin shows unusual differences. *Proteins: Struct. Funct. Genet.* **19**, 302–309.

Mangum, C. P. (1983). On the distribution of lactate sensitivity among the hemocyanins. *Mar. Biol. Letters*, **4**, 139–149.

Mangum, C. P. & Burnett, L. E., Jr (1986). The CO_2 sensitivity of the hemocyanins and its relationship to Cl^- sensitivity. *Biol. Bull.* **171**, 248–263.

Mangum, C. P., Booth, C. E., DeFur, P. L., Heckel, N. A., Henry, R. P., Oglesby, L. C. & Polites, G. (1976). The ionic environment of hemocyanin in *Limulus polyphemus*. *Biol. Bull.* **150**, 453–467.

Markl, J. & Decker, H. (1992). Molecular structure of the arthropod hemocyanins. In *Blood and Tissue Oxygen Carriers* (Mangum, C. P., ed.), pp. 325–363, Springer-Verlag, New York.

McPherson, A. (1990). Current approaches to macromolecular crystallization. *Eur. J. Biochem.* **189**, 1–23.

Pflugrath, J. W. & Messerschmidt, A. (1986). MADNES user's guide, Max-Planck institute für biochemie, Martinsried, Federal Republic of Germany.

Ramakrishnan, C. & Ramachandran, G. N. (1965). Stereochemical criteria for polypeptide and protein chain conformation. *Biophys. J.* **5**, 909–933.

Read, R. J. (1986). Improved Fourier coefficients for maps using phases from partial structures with errors. *Acta Crystallog. sect. A*, **42**, 140–149.

Riggs, A. F. & Wolbach, R. A. (1956). Sulfhydryl groups and the structure of hemoglobin. *J. Gen. Physiol.* **39**, 585–605.

Strynadka, N. C. J. & James, M. N. G. (1989). Crystal structures of the helix-loop-helix calcium-binding proteins. *Annu. Rev. Biochem.* **58**, 951–998.

Sullivan, B., Bonaventura, J. & Bonaventura, C. (1974). Functional differences in the multiple hemocyanins of the horseshoe crab, *Limulus polyphemus* L. *Proc. Natl Acad. Sci. USA*, **71**, 2558–2562.

Thamann, T. J., Loehr, J. S. & Loehr, T. M. (1977). Resonance Raman study of oxyhemocyanin with unsymmetrically labeled oxygen. *J. Am. Chem. Soc.* **99**, 4187–4189.

Towle, D. W., Mangum, C. P., Johnson, B. A. & Mauro, N. A. (1982). The role of the coxal gland in ionic, osmotic, and pH regulation in the horseshoe crab *Limulus polyphemus*. In *Physiology and Biology of Horseshoe Crabs: Studies on Normal and Environentally Stressed Animals* (Bonaventura, J., Bonaventura, C. & Tesh, S., eds), pp. 147–172, Alan R. Liss, Inc. New York.

Van Bruggen, E. F. J., Schutter, W. G., Van Breemen, J. F. L., Bijlholt, M. M. C. & Wichertjes, T. (1982). Arthropodan and molluscan haemocyanins. In *Electron Microscopy of Proteins* (Harris, M., ed.), pp. 11–28, Academic Press, New York.

Van Heel, M. & Dube, P. (1994). Quaternary structure of

multihexameric arthropod hemocyanins. *Micron*, **25**, 387–418.
Van Holde, K. E. & Miller, K. I. (1982). Haemocyanins. *Quart. Rev. Biophys.* **15**, 1–129.
Volbeda, A. & Hol, W. G. J. (1989). Crystal structure of hexameric haemocyanin from *Panulirus interruptus* refined at 3.2 Å resolution. *J. Mol. Biol.* **209**, 249–279.

Edited by I. A. Wilson

(Received 6 February 1996; received in revised form 19 July 1996; accepted 26 July 1996)